DUJASE Vol. 3(1) 7-13, 2015 (January)

Study on the Effect of Bi_2O_3 Additive on the Microstructure, Structural and Magnetic Properties of $Ni_{0.35}Cu_{0.15}Zn_{0.5}$ Ferrite Sintered at 1100^0C

Md. Fazlul Huq[1], D. K. Saha[2] and Zahid Hasan Mahmood[3].

[1]*Department of Nuclear Engineering, University of Dhaka, Dhaka-1000, Bangladesh.*

[2]*Materials Science Division, Atomic Energy Centre Dhaka, Dhaka- 1000, Bangladesh.*

[3]*Department of Electrical and Electronic Engineering, University of Dhaka, Dhaka - 1000, Bangladesh.*

Email: fazlul.huq@du.ac.bd

Received on 23. 05. 2012. Accepted for publication on 14.07. 2014.

Abstract

The effect of variation of addition of Bi_2O_3 (0 wt.%, 1 wt.%, 2 wt.% and 3 wt.%) on the microstructure, structural and magnetic properties of $Ni_{0.35}Cu_{0.15}Zn_{0.50}Fe_2O_4$ has been reported. The Scanning Electron Micrograph (SEM) of the samples reveals that the grain size increases with increasing additive up to 2 wt.% addition. Above 2 wt.% addition, no significant change in grain size is evident. The X-Ray Diffraction (XRD) pattern confirms the crystallization of the samples in single-phase cubic spinel structure. The lattice constant of $Ni_{0.35}Cu_{0.15}Zn_{0.50}Fe_2O_4$ increases gradually with increasing Bi_2O_3 content up to 2 wt.% addition. A further addition shows decrease in lattice constant. Again, the addition of Bi_2O_3 produced a thick liquid phase layer at the grain boundaries and retarded mass transfer during sintering. Thus the X-ray diffraction peaks exhibited reduced intensity. Bi_2O_3 promoted grain growth via liquid phase sintering, and the addition of the optimum content could enhance the density of the sample and reduces its porosity. The Energy Dispersive X-ray Spectroscopy (EDS) analysis ensures proper doping profile of the prepared specimens. The Curie temperature has been investigated from temperature dependent permeability analysis. Undoped $Ni_{0.35}Cu_{0.15}Zn_{0.50}Fe_2O_4$ shows Curie temperature of 239^0C and increases with increase in doping percent of Bi_2O_3. 3 wt.% doping shows Curie temperature of 245^0C.

Keywords: XRD, SEM, EDS, Spinel Structure, Porosity, Curie Temperature (T_c), Permeability.

1. Introduction

Study of the polycrystalline spinel ferrite has great importance because of its extensive application in many electronic devices. Due to their amazing magnetic and electric properties, spinel ferrites have become a subject of both theoretical and experimental investigation for application purposes [1–5]. They are preferred because of their high permeability and saturation magnetization in the radio-frequency (RF) region, high electrical resistivity, mechanical hardness and chemical stability. Ferrites are also useful to prevent and eliminate RF interference to audio systems.

Miniaturized components are highly in demand, such as, portable computer (PC), liquid crystal display (LCD), plasma display panel (PDP) and personal digital assistant (PDA) etc. The circuits of these equipments have to consider miniature dc–dc converters, inductors for filters and signal amplifying power inductors. Therefore, it is necessary to realize the miniaturization of electromagnetic components. At present, MnZn ferrites have been widely used in the mini dc–dc converters and inductors [6]. However, NiCuZn ferrites can offer better miniaturization prospects, since they have high electrical resistivity and can miniaturize magnetic components without a bobbin [7–10].

Because of the AB_2O_4 crystal structure of Ni-Cu-Zn ferrite, they show various magnetic properties depending on chemical composition and cation distribution in tetrahedral A and octahedral B sites [11]. Several researchers have prepared Ni-Cu-Zn ferrite [12-16]. Zn^{2+} is used to improve electromagnetic properties as well as densification in the ferrite. It is substituted in spinel ferrite to improve magnetization [17]. It also lowers magnetostriction and anisotropy in ferrites [18]. Goev et al. [19] stated that initial permeability increased and hysteresis loss decreased with increasing Zn concentration in $Ni_{0.85-y}Cu_{0.15}Zn_yFe_2O_4$ ferrite. Cu is conventionally used to improve densification as well as electromagnetic properties [20].

Besides, the chemical composition [21], sintering process [21–25], the additive are also important here, since it influences the microstructure and magnetic properties of NiCuZn ferrites. Recently, additives with a low melting point, such as PbO [22, 23], V_2O_5 [24–28], B_2O_3 [29] and Bi_2O_3 [30–39], have been reported to obtain NiZn ferrites of high performance.

Here in the present research work, we have investigated the effect of Bi_2O_3 additive on microstructure, crystal structure, densification and magnetic properties of $Ni_{0.35}Cu_{0.15}Zn_{0.5}$ ferrite sintered at 1100^0C.

2. Experimental Detail

The $Ni_{0.35}Cu_{0.15}Zn_{0.50}Fe_2O_4$+ x% wt. of Bi_2O_3 (where x= 0, 1, 2 and 3) samples were synthesized using the standard solid-state reaction technique. Powders of NiO(99.99%), CuO(99.99%), ZnO(99.99%), Fe_2O_3(99.99%) and Bi_2O_3(99.99%) are available at Atomic Energy Centre, Dhaka, which are collected from E. Mark of Germany were

used as raw materials. Stoichiometric amounts of required powders were mixed by hand milling and ball milling.

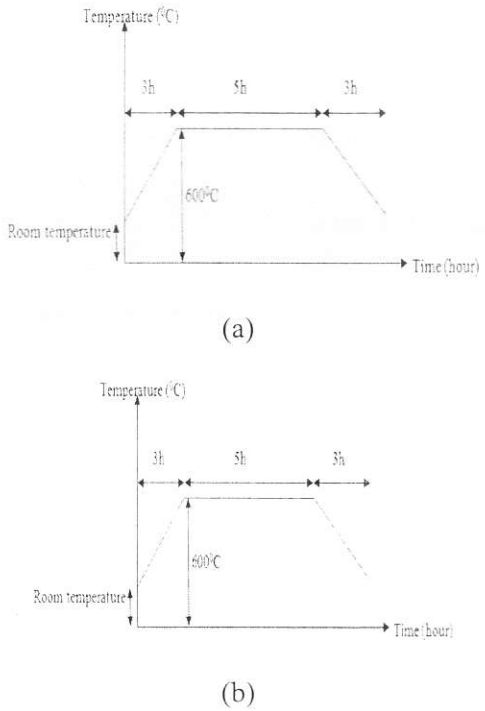

Fig. 1: Time vs. temperature profile for (a) pre-sintering and (b) sintering.

The mixed and dried powder was pressed into disc shape. The disc shaped sample was pre-sintered using NABERTHERM ($300^0C - 3000^0C$) furnace with temperature profile as shown in fig. 1(a). The pre-sintered sample is then powdered and reshaped into desired shape and then sintering is performed with temperature profile as shown in fig. 1(b). The samples were polished and then thermal etching was performed. The morphological properties and EDS were studied by Scanning Electron Microscope named "FEI Quanta Inspect", Model is S-50.

To study the crystalline phases of the prepared samples, X-ray diffraction (XRD) pattern has been recorded at room temperature with CuK_α radiation of wavelength $\lambda = 1.54178\ A^0$ with primary beam power of 40 kV and 30 mA using a Philips PW3040 X'Pert PRO X-ray diffractometer. Resolution of the scan was set to 0.01^0 with a sampling pitch of 0.02° and time for each step data collection was 1.0 sec. A 2θ scan was taken from 10° to 90° to get possible fundamental peaks where Ni filter was used to reduce CuK_β radiation. All the data of the samples were analyzed using computer software "X' PERT HIGHSCORE".

The temperature-dependent initial permeability was measured using WAYNE KERR IDUCTANCE ANALYZER 3255B, a small oven and a thermocouple based thermometer at a constant frequency (100 kHz). We used AC signal of 100 mV of a sinusoidal wave. The Curie temperature (T_c) of the samples was determined from the temperature-dependent initial permeability as a function of temperature measurements. Generally a heating of $\approx 2^0C$ / min was used. Near the Curie temperature heating rate was less than 1^0C / min.

3. Result and Discussion

XRD-Pattern

Eight fundamental reflections from the planes of (111), (220), (311), (222), (400), (422), (511) and (440) are evident from the fig. 2 which strongly determines the cubic spinel structure[40]. These peaks correspond to spinel phases. Thus the analysis of XRD patterns indicated that the studied $Ni_{0.35}Cu_{0.15}Zn_{0.50}Fe_3O_4 + xBi_2O_3$ ferrite samples with x = 0, 1, 2 and 3 wt. % has single-phase cubic spinel structureswith no presence of undesired phases.

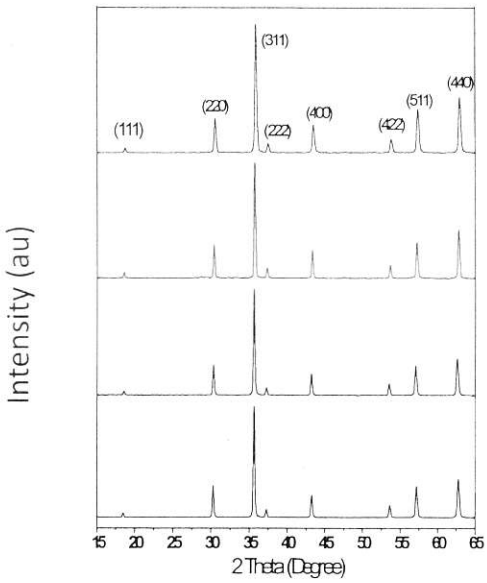

Fig. 2: Comparison of XRD patterns of $Ni_{0.35}Cu_{0.15}Zn_{0.50}Fe_3O_4 + x\ Bi_2O_3$ ferrite samples with x= 0, 1, 2 and 3 wt. % respectively.

With increasing wt.% of Bi_2O_3 the intensity becomes gradually weaker. It could be interpreted that, the excessive content of Bi_2O_3 produces a thick liquid-phase and retards the grain growth, resulting in a decrease in intensity of the diffraction peaks [41].

Lattice Parameters

The values of the lattice parameter obtained from each plane are plotted against Nelson-Riley function [42] $F(\theta) = \frac{1}{2}[\cos^2\theta/\sin\theta + \cos^2\theta/\theta]$, where θ is the Bragg's angle. The values of lattice parameters were then estimated from the extrapolation of these lines to $F(\theta) = 0$ or, $\theta = 90^0$.

Extrapolation provides lattice parameters $8.3945\ A^0$, $8.3954\ A^0$, $8.3968\ A^0$ and $8.3895\ A^0$ respectively for 0 wt. %, 1 wt. %, 2 wt. % and 3 wt. % addition of Bi_2O_3 with $Ni_{0.35}Cu_{0.15}Zn_{0.50}Fe_3O_4$. Thus the lattice parameter increases

with increase of Bi_2O_3 content within $Ni_{0.35}Cu_{0.15}Zn_{0.50}Fe_3O_4$ up to 2 wt. %. This is very much expected since the ionic radius of Bi (1.17 Å) is higher than ionic radius of Ni (0.83 Å), Cu (0.87 Å) and Zn (0.88 Å) [43]. Thus addition Bi_2O_3 increases the lattice parameter.

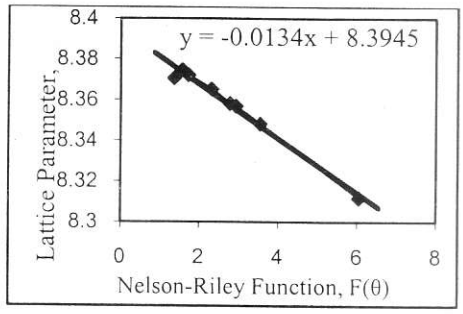

(a)

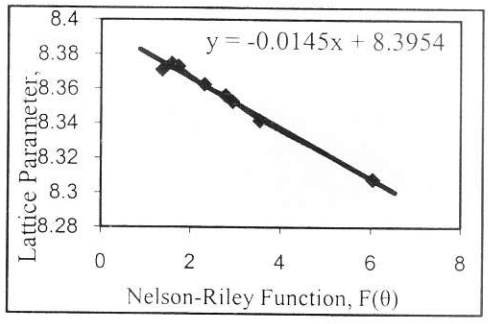

(b)

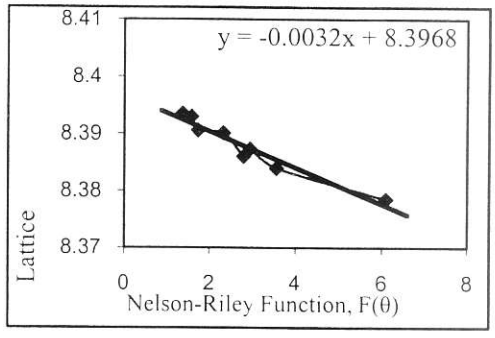

(c)

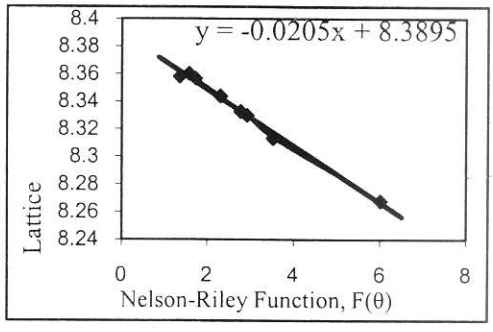

(d)

Fig. 3: Lattice parameter, a Vs. Nelson-Riley function plot of $Ni_{0.35}Cu_{0.15}Zn_{0.50}Fe_3O_4$+x Bi_2O_3 sample with, (a) x= 0 wt. %, (b) x = 1 wt. %, (c) x = 2 wt. % and (d) x = 3 wt. %.

In case of 3 wt. % addition of Bi_2O_3 with $Ni_{0.35}Cu_{0.15}Zn_{0.50}Fe_3O_4$ different situation arises. Here, the value of lattice parameter falls. In fact, Bi_2O_3 provide sintering aid. Ni-Cu-Zn ferrite with a only 0.8 wt. % addition of Bi_2O_3 shows a reduction in sintering temperature up to 150^0C [44]. When 3 wt. % of Bi_2O_3 is added then reduction in sintering is very high. Thus at sintering temperature of 1100^0C may be over sintering takes place and thus lattice parameter decreases.

Density and Porosity

The x-ray density also called theoretical density is determined using,

$$\rho_x = \frac{ZM}{Na^3} \quad \ldots \ldots \ldots \ldots \quad (1)$$

where, N is Avogadro's number ($6.023 \times 10^{23} mol^{-1}$), M is the molecular weight and Z is the number of atoms per unit cell, which is 8 for the spinel cubic structure.

Bulk density is calculated as the ratio of mass to weight. Calculated bulk density then plotted against wt.% addition of Bi_2O_3 in Fig. 4(b).

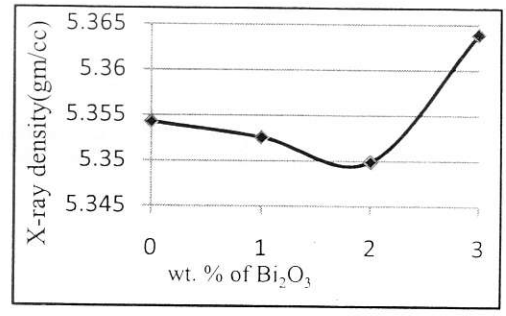

(a)

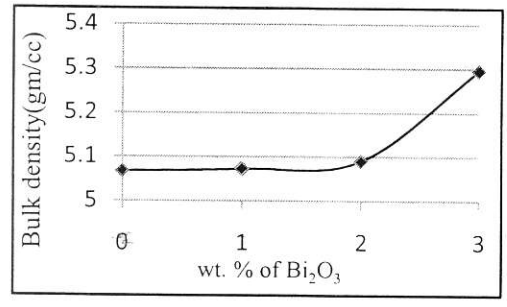

(b)

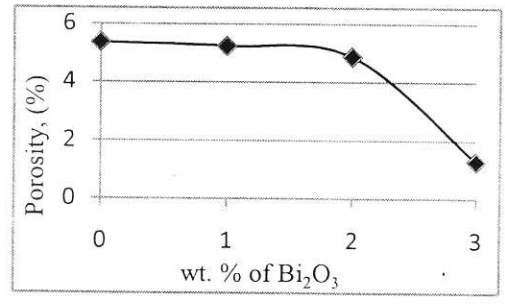

(c)

Fig. 4: Variation of (a) theoretical density, (b) bulk density and (c) porosity for different (0, 1, 2 and 3) wt. % addition of Bi_2O_3 with $Ni_{0.35}Cu_{0.15}Zn_{0.50}Fe_3O_4$.

The addition of Bi_2O_3 additive enhances the mass transfer and sintering via liquid phase to get higher density at the same temperature. Because the Bi_2O_3 additive remains liquid when the temperature is over 820^0C, it forms low melting eutectics. This phenomenon agrees with the results of XRD measurement. The improvement in density of Bi-doped samples could be attributed to the following reasons: (1) the main reason is the improvement in the rate of grain growth due to the formation of liquid phase and (2) the secondary reason is the higher density of Bi_2O_3 (8.9 g cm−3) in comparison with $Ni_{0.35}Cu_{0.15}Zn_{0.50}Fe_3O_4$ ferrite density. Wang et al have proved that the formation of the Pi_2O_3 liquid phase could be attributed to the densification of NiZn ferrite at a lower temperature through particle re-arrangement, solution-reprecipitation and solid skeleton process. For the similar reasons porosity on the other hand gradually decreases with increase in wt. % doping of Bi_2O_3.

Porosity P is determined using,

$$P = (1 - \frac{\rho_B}{\rho_X}) \text{ X } 100\% \ldots\ldots\ldots(2)$$

where, ρ_B is the bulk density measured by usual mass volume ratio and ρ_X is the theoretical density or X-ray density.

SEM Micrograph Analysis

The microstructures of $Ni_{0.35}Cu_{0.15}Zn_{0.50}Fe_3O_4$ + x Bi_2O_3 (x= 0, 1, 2 and 3) sintered at 1100^0C has been represented in Fig. 5. Figure shows the variation of grain size with doping percentage. For pure $Ni_{0.35}Cu_{0.15}Zn_{0.50}Fe_3O_4$ the grain size is relatively small as shown in Fig. 5(a). Fig. 5(b) and Fig. 5(c) shows gradual increase in grain size that corresponds to 1wt. % and 2 wt. % addition of Bi_2O_3. In case of 3 wt. % addition of Bi_2O_3 no significant change in grain size occurs which is evident in Fig. 5(d). This is may be due the presence of excessive amount of Bi_2O_3, of which melting point is only 820^0C whereas sintering temperature is 1100^0C. Thus this excessive amount of Bi_2O_3 at such high sintering temperature creates a liquid environment which prevents further increase in grain size.

Again for the samples with small grains, pores are found usually at the grain boundary. For the samples with large grains, the majority of the pores are trapped inside the grains at large distance from the grain boundary, which affects the value of permeability, density dielectric constant and resistivity.

This study postulates different mechanisms pertaining to the grain growth in the case of NiCuZn ferrites which depends on the amount of liquid phase present in the system [31-33, 45].

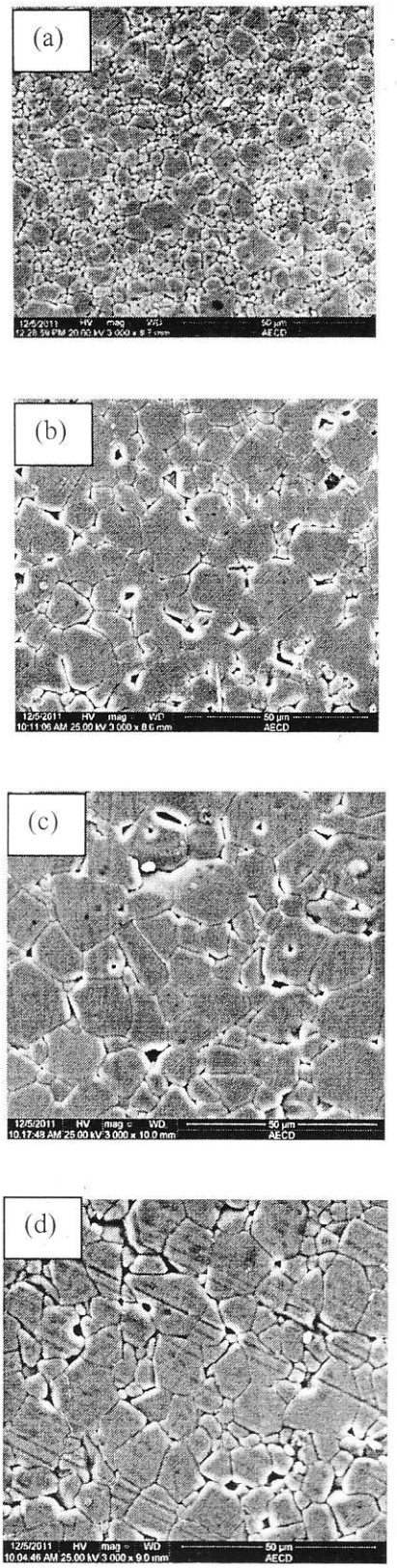

Fig. 5: SEM micrograph of $Ni_{0.35}Cu_{0.15}Zn_{0.50}Fe_3O_4$ + x wt. % Bi_2O_3 sintered at 1100^0C, where, (a) x = 0, (b) x = 1, (c) x = 2 and (d) x = 3.

EDX Analysis

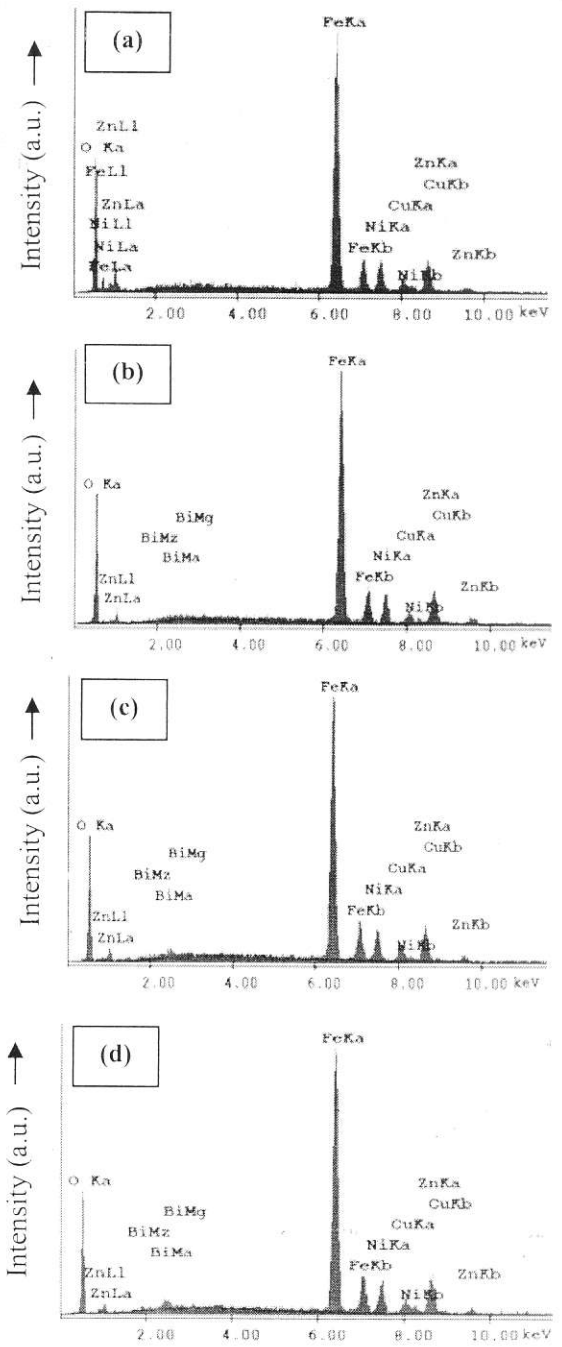

Fig. 6: EDX analysis of $Ni_{0.35}$ $Cu_{0.15}$ $Zn_{0.50}$ Fe_3O_4 + x wt. %Bi_2O_3 sintered at 1100^{0}C, where, (a) x = 0, (b) x = 1, (c) x = 2 and (d) x = 3.

The EDX analysis images are represented in Fig. 6. Fig. 6(a) shows no presence of Bi content which ensures 0 wt. % addition of Bi_2O_3 in this sample as expected. The image provided by SEM does not include any scaling in vertical axis but provide quantified data. The quantified data for Bi content provided by SEM are represented in table 1.

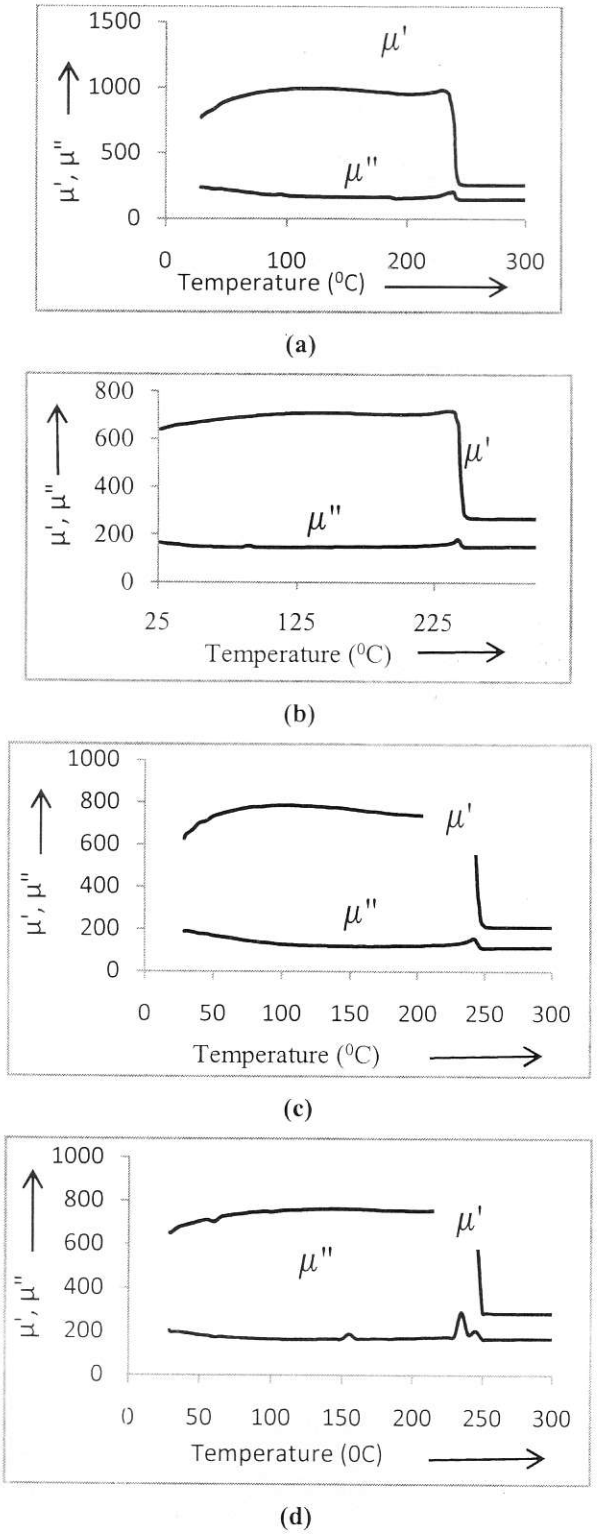

Fig. 7: Temperature dependence of permeability for $Ni_{0.35}Cu_{0.15}Zn_{0.50}Fe_3O_4$ + x wt. %Bi_2O_3 sintered at 1100^{0}C, where, (a) x = 0, (b) x = 1, (c) x = 2 and (d) x = 3.

Table 1: Wt. % and atomic % presence of Bi content in $Ni_{0.35}Cu_{0.15}Zn_{0.50}Fe_3O_4 + x\ Bi_2O_3$ for x= 0, 1, 2 and 3 wt. %.

Wt. % of Bi_2O_3, (x) in $Ni_{0.35}Cu_{0.15}Zn_{0.50}Fe_3O_4 + x\ Bi_2O_3$	Wt. % of Bi	Atomic % of Bi
0	0	0
1	0.63	0.16
2	0.81	0.20
3	1.11	0.28

The table ensures the proper doping of the sample with Bi_2O_3.

Temperature Dependent Permeability

The variation of real and imaginary permeability with variation of temperature are depicted in Fig. 7. The figure reveals that, highest permeability is found with pure $Ni_{0.35}Cu_{0.15}Zn_{0.50}Fe_3O_4$. For each % of doping, frequency dependent real permeability up to Curie temperatures are nearly same and are less than 0 % doping.

Curie Temperature

From curves of temperature dependent permeability (Fig. 7) Curie temperatures are determined. Determined Curie temperatures are given in Table 2.

Table 2: Curie temperatures for $Ni_{0.35}Cu_{0.15}Zn_{0.50}Fe_3O_4$ +x wt. % of Bi_2O_3 (x= 0, 1, 2 and 3) sintered at 1100^0C.

Wt. % of Bi_2O_3, (x) in $Ni_{0.35}Cu_{0.15}Zn_{0.50}Fe_3O_4 + x\ Bi_2O_3$	Determined Curie Temperature, T_c (^{0}C)
0	239
1	243
2	243
3	245

The table clearly shows that, with increase in doping % of Bi_2O_3 the Curie temperature of the samples are increases.

4. Conclusions

In investigating the grain growth, densification and magnetic properties of $Ni_{0.35}Cu_{0.15}Zn_{0.50}$ ferrites doped with different contents of Bi_2O_3 shows that, addition of Bi_2O_3 additive, to $Ni_{0.35}Cu_{0.15}Zn_{0.50}Fe_3O_4$, due to its liquid phase sintering, enhances the diffraction intensity while excessive (>1 wt.%)content of Bi_2O_3 produces a thick liquid phase layer at the grain boundaries and retards mass transfer during sintering. Thus the X-ray diffraction peaks exhibit reduced intensity. Addition of Bi_2O_3 does not introduce any phase mismatching within the crystal structure. Bi_2O_3 promotes grain growth via liquid phase sintering and addition of Bi_2O_3 enhances density and reduces porosity. Microstructure study reveals that the grain size increases with increasing Bi_2O_3 up to 2 wt.% addition. A further addition does not show any significant increase in grain size. Again in case of small sized grain, the pores are relatively high and are distributed at the boundary of the grain. On the other hand, number of pores gradually decreases with increasing grain size and are distributed mostly within the grain. EDX analysis clearly ensures proper doping of the dopant. Temperature dependent permeability curves shows that, below Curie temperature, undoped $Ni_{0.35}Cu_{0.15}Zn_{0.50}$ ferrite shows relatively higher permeability than doped one. But with increasing doping percent of Bi_2O_3, Curie temperature gradually increases.

Acknowledgement

The authors are thankful to Materials ScienceDivision, Atomic Energy Centre Dhaka, Dhaka-1000,Bangladesh, for extending experimental facilities.

References

1. J.M. Hastings, L.M. Corliss, Phys. Rev. 102 (6) (1956) 1460.
2. J.M. Hastings, L.M. Corliss, Rev. Mod. Phys. 25 (1) (1953) 114.
3. B.N. Brockhouse, L.M. Corliss, J.M. Hastings, Phys. Rev. 98 (6) (1955) 1721.
4. W. Schiessl, W. Potzel, H. Karzel, M. Steiner, G.M. Kalvius, A. Martin, M.K. Krause, I. Halevy, J. Gal, W. Schafer, G. Will, M. Hilberg, R. Wappling, Phys. Rev. B 53 (14) (1996) 9143.
5. Y. Yamada, K. Kamazawa, T. Tsunoda, Phys. Rev. B 66 (2002) 064401.
6. Matsuo Y, Mochizuki T, Ishikura M and Sasaki 1996 J. Magn. Soc. Japan 20 429.
7. Araki T and Morinaga H 1992 Proc. 6th Int. Conf. on Ferrites ICF-6 (Kyoto and Tokyo, Japan) p 1185.
8. Lebourgeois R, Perriat P and Labeyrie M 1992 Proc. 6th Int. Conf. on Ferrites ICF-6 (Kyoto and Tokyo, Japan) p 1159.
9. Matsuo Y, Inagaki M, Tomozawa T and Nakao F 2001 IEEE Trans. Magn. 37 2359.
10. Kondo K, Chiba T, Yamada S and Otsuki E 2000 J. Appl. Phys. 87 6229.
11. R. Peelamedu, C. Grimes, D. Agrawal, R. Roy, J. Mater. Res. 18 (10) (2003) 2292.
12. S. Yan, J. Geng, L. Yin, E. Zhou, J. Magn. Magn. Mater. 277 (1-2) (2004) 84.
13. Z. Yue, L. Li, J. Zhou, H. Zhang, Z. Gui, Mat. Sci. Engg. B 64 (1999) 68.
14. Z. Yue, L. Li, J. Zhou, H. Zhang, Z. Gui, J. Magn. Magn. Mater. 233 (2001) 224.
15. K. O. Low, F. R. Sale, J. Magn. Magn. Mater. 246 (2002) 30.
16. J. G. Koh, J. Kore. Phys. Soc. 44 (6) (2004) 1504.
17. J. Smit, H. P. J. Wijn, Ferites, John Wiley & Sons, New York (1959).

18. N. R. Reddya, M. V. Ramanaa, G. Rajithaa, E. Rajagopala, K.V. Sivakumara, V. R. K. Murthy, J. Magn. Magn. Mater. 292 (2005) 159.
19. G. Goev, V. Masheva, L. Ilkov, D. Nihtianova, M. Mikhov, Proceedings of the fifth General Conference of the Balkan Physical Union BPU-5 (2003) 687.
20. S. Modak, M. Ammar, F. Mazaleyrat, S. Das, P. K. Chakrabarti, J. All. Compd. 473(1-2) (2009) 15.
21. Su H, Zhang H W, Tang X L, Jing Y L and Liu Y L 2007 J. Magn. Magn. Mater. 310 17.
22. Jean J H and Lee C H 1999 J. Am. Ceram. Soc. 82 343.
23. Rezlescu N, Sachelarie L, Rezlescu E, Sava C L and Popa P D 2003 Ceram. Int. 29 107.
24. Rao B P, Kim C O and Kim C G 2007 Mater. Lett. 61 1601.
25. Jean J H and Lee C H 2001 Japan. J. Appl. Phys. 40 2232.
26. Lebourgeois R et al 2007 J. Magn. Magn. Mater. 312 328.
27. Mirzaee O, Shafyei A, Golozor M A and Shokrollahi H 2008 J. Alloys Compounds 461 312.
28. Mirzaee O, Golozar M A and Shafyei A 2008 Mater. Charact. 59 638.
29. Yuksel B et al 2008 J. Magn. Magn. Mater. 320 714.
30. Kim H T and Im H B 1982 IEEE Trans. Magn. 18 1541.
31. Hendricks C R, Amarakoon V W R and Sullivan D 1991 Ceram. Bull. 70 817.
32. Wang S F et al 2000 J. Magn. Magn. Mater. 220 129.
33. Jean J H and Lee C H 1999 Japan. J. Appl. Phys. 38 3508.
34. Topfer J et al 2006 Int. J. Ceram. Technol. 3 455.
35. Su H, Zhang H W and Tang X L 2005 Mater. Sci. Eng. B 117 231.
36. Y. H. Wang, S. F. Wang, Int. J. Inorg. Mat. 3 (2001) 1189.
37. J. Y. Hsu, W. S. Ko, H. D. Hen, C. J. Chen, IEEE Trans. Mag. 30 (6) (1994) 4875.
38. S. F. Wang, Y. R. Wang, T. C. K. Yang, C. F. Chen, C. A. Lu, C. Y. Huang, J. Magn. Magn. Mater. 220 (2000) 129.
39. J. Jeong, H.Y. Han, C.B. Moon, J. Mat. Sci. Mat. In Elect. 15 (5) (2004) 303.
40. S. J. So and C. B. park, J. Korean Phys. Soc. 38, 417 (2001).
41. Ke Sun, ZhongwenLan, Zhong Yu, Lezhong Li, Jiaomin Huang and Xiaoning Zhao, 2008 J. Phys. D: Appl. Phys. 41 235002.
42. J. B. Nelson, D. P. Riley, Proc. Phys. Soc. London 57 (1945) 160.
43. L. John Berchamans, R. KalaiSelvan, P.N. Selva Kumar and C.O. Augustin, J. Magn. Magn Mater. 279 (2004)103.
44. D. K. Saha and M. A. Hakim, J. of Nuclear Science and Applications, 15 (2006)33.
45. Drofenik M, Znidarsic A and Makovec D 1998 J. Am. Ceram. Soc. 81 2841.